Inorganic Chemistry

Article

pubs.acs.org/IC

On the Nature of the Structural and Magnetic Phase Transitions in the Layered Perovskite-Like $(CH_3NH_3)_2[Fe^{II}Cl_4]$

Jing Han,[†] Sadafumi Nishihara,[†,‡] Katsuya Inoue,*[,†,‡] and Mohamedally Kurmoo*[,§]

[†]Department of Chemistry, Graduate School of Science, Hiroshima University, 1-3-1, Kagamiyama, Higashi Hiroshima, Hiroshima 739-8526, Japan

[‡]Institute for Advanced Materials Research, Hiroshima University & Natural Science Center for Basic Research and Development, 1-3-1, Kagamiyama, Higashi Hiroshima, Hiroshima 739-8526, Japan

[§]Institut de Chimie de Strasbourg, CNRS-UMR 7177, Université de Strasbourg, 4 rue Blaise Pascal, 67070 Strasbourg, France

Supporting Information

ABSTRACT: In view of renewed interest in multiferroic for molecular systems, we re-examine the structural and magnetic properties of the potentially ferroic layered perovskite-like $(CH_3NH_3)_2[Fe^{II}Cl_4]$ due to its high-temperature magnetic ordering transition. The structures from several sets of diffraction data of single crystals consist of square-grid layers of corner-sharing $FeCl_6$ octahedra and changes from the high-symmetry $I4/mmm$ (T > 335 K) to the low-symmetry $Pccn$ (T < 335 K). In the former the iron and bridging chlorine atoms are within the layer and the organic cations sit in the middle of each square grid, while in the latter the octahedra are tilted in pairs, two in and two out, progressively by up to 12° and the nitrogen atoms follow their motion to be nearer to the two-in pairs. Crystals are stable up to 450 K and display three phase transitions, two structural at 332 and 233 K and one magnetic at 95 K. The temperature dependences of the dc magnetization (zero-field and field-cooling modes) in different applied fields (10−10 000 Oe) on several aligned single crystals independently reveal a hidden-canted antiferromagnetic ground state of at least four sublattices and not the reported canted antiferromagnetic ground state. A metamagnetic critical field of only 200 Oe transforms it to a canted antiferromagnet. The estimated canting angle is 1.4° in zero field, and it folds to ca. 2.8° in a field of 50 kOe at 2 K. The easy axis is along 010, the hard axis is along 100, and the intermediate and canting axis is 001. Using the available extracted parameters the phase diagram has been constructed. This study provides evidence of a complex and intricate manifestation of the orientation, temperature, and field dependence of the interplay between anisotropy and coherent lengths, which would need further studies.

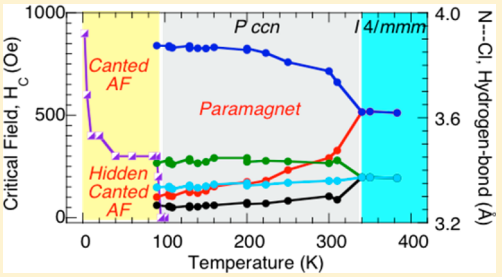

INTRODUCTION

Interest in perovskite is experiencing a revival due to recent observation of ferroelectricity and magnetic order.[1−9] Multiferroics are being developed for compounds having the perovskite structure of general formula ABO_3[1,2] for reasons related to the deformation brought about by the presence of the lone pair on the A-site metal ions such as Bi^{3+}, for example, $BiFeO_3$ and $BiMnO_3$. Further interesting physics arrived with the presence of rare-earth magnetic moment carriers at the A site of manganites, for example, $TbMnO_3$. Thus, ferroelectricity and ferromagnetism can be realized within the same temperature range. More recent developments have focused on metal−organic frameworks having the diamond network, $M_3(HCOO)_3$·solvent,[3] and the 3D perovskite structure, $(CH_3)_2NH_2$ $M(HCOO)_3$,[4] following their syntheses and structural and magnetic properties studies by Wang et al. and Gao et al. Kobayashi et al. first reported the dielectric properties of the 3D diamond metal−formate framework, $M_3(HCOO)_3$·solvent,[5] which was followed by Cheetham et al. by observation of ferroelectricity in the 3D perovskite metal−formate frameworks.[6] The dielectricity is associated with the order−disorder of the solvent in the diamond networks and of the organic cations in the perovskites. While these 3D materials exhibit ferroelectricity and canted antiferromagnetism (CAF), the respective transition temperatures are very far apart, ca. 200 K for the former and below 30 K for the latter. Since then several groups have reported similar observations, and some theoretical works have also followed.[7−9]

In view of these major developments, especially the observation of spiral spin orders,[2] and our long-term interest in chiral materials,[10] we set out to study the family of layered perovskite-like $A_2M^{II}X_4$,[11] where A is an alkyl or aryl ammonium, M is a divalent open-shell transition metal to provide the magnetism, and X is a halogen.[12−15] These materials have been of major interest since the early 1970s due to the long-range magnetic ordering of the moments at fairly high temperatures, although they are layered with interlayer spacings of up to 30 Å in some cases. Following recent observation of ferroic transition in analogous layered perovskite-like copper by Palstra et al. and iron by Xiong et al.[16] and the theoretical investigation of Oguchi et al.,[17] our present

Received: October 17, 2013
Published: January 28, 2014

   dx.doi.org/10.1021/ic402535u | Inorg. Chem. 2014, 53, 2068−2075

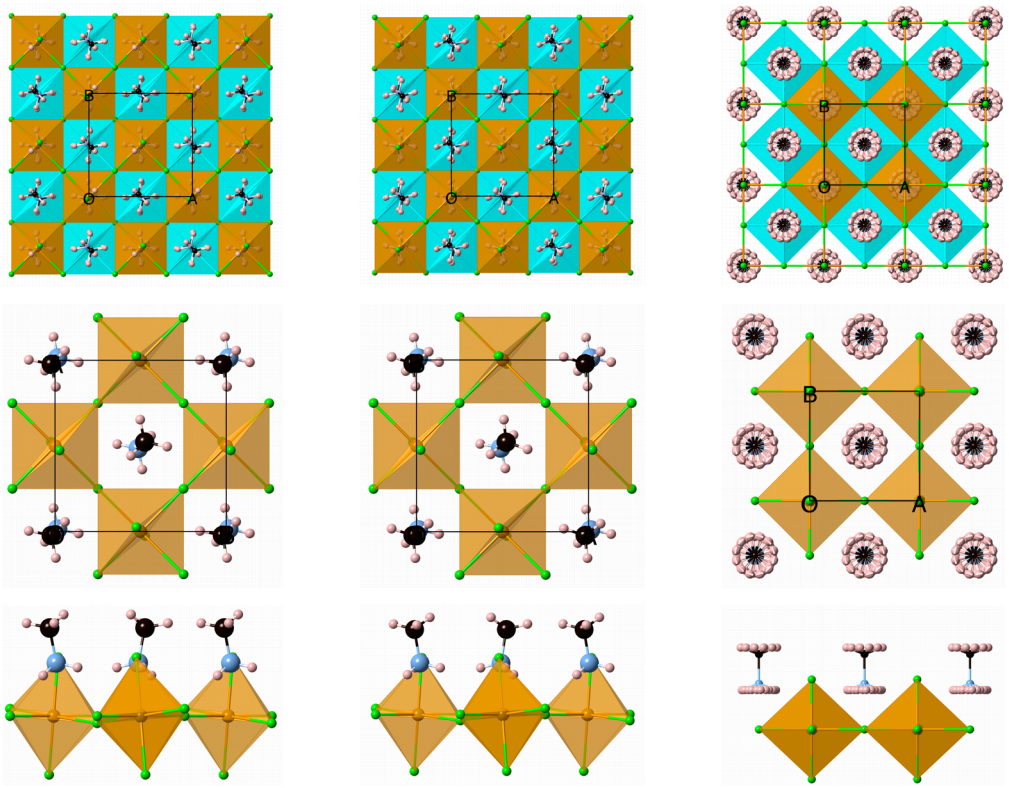

Figure 1. Structures of MAFC at 90 (left column), 223 (center column) and 383 K (right column) with projection along the *c* axis (top row) showing the staggered stacks in brown and cyan, the docking of the organic cations above and below the inorganic layer (middle row), and view along the layer showing the tilting of the octahedra and the cations (bottom row).

target for the work here is the first member of the iron series, $(CH_3NH_3)_2FeCl_4$ (MAFC).[18−25]

Being an easy material to prepare as large single crystals and having a magnetic transition temperature above liquid nitrogen temperature, MAFC was very popular for various studies. X-ray and neutron diffractions established the layered structures, and from lattice parameter measurements the structural phase transitions tetragonal−orthorhombic−tetragonal were demonstrated.[20] For all phases the layered structure was retained and the layer surface, described as a washboard, changes slightly due to tilting of the octahedra. However, there is a lack of full structure determinations at various temperatures. Here, we explore the crystal chemistry of MAFC by measuring the lattice parameters and determination of the crystal structures at several temperatures from 100 to 400 K. Our results on five independent crystals indicate that the structure does not follow the Heger et al. proposed family tree for these layered perovskites based on two different mechanisms.[20] The first is a reduction of rotational symmetry (t2 for translationgleich) and second is a reduction of translational symmetry (k2 for klassengleich). Elastic, DSC, and optical birefringence measurements confirm these phase transitions. Magnetic measurements have been performed using Gouy and Faraday balances, a vibrating-sample magnetometer, the induction technique, and an ac susceptometer in fields usually from ca. 1 to 12 kOe.[21−25] While some studies were performed from 300 to 80 K, several were carried out down to 4 K. Both powdered samples and oriented single crystals have been studied.

Previous studies have established a magnetic phase transition between 92 and 96 K, depending on reports, and the ground state is reported to be a CAF,[25] though considerable field dependence has been noted below the Néel temperature (T_N).[22] It is also concluded that the moments lie in the plane, that is it is an easy-plane magnet. The lack of measurements in low fields has hampered the elucidation of the true ground state. The present study using a low field of 50 Oe, temperature from 400 to 2 K for a field aligned along the three crystallographic axes, and zero-field-cooling and field-cooling modes reveals the intricate manifestation of hidden canting in zero field and a metamagnetic (MM) transition in less than 300 Oe from a fully compensated antiferromagnetic (AF) ground state to a CAF one. Our results confirm the *XY* dimensionality for the magnetism as found from the critical exponent extracted from the temperature dependence of the Mössbauer spectra,[23,26] in contrast to Ising inferred from the heat capacity measurements.[27]

EXPERIMENTAL SECTION

Synthesis. Since the product and reactants are hygroscopic and air sensitive, all steps were carried out in inert atmosphere. MAFC was obtained by mixing methanol solutions of methyl ammonium chloride, $(CH_3NH_3)Cl$, and $FeCl_2{\cdot}4H_2O$ in a 2:1 molar ratio. Plates of pale yellow to orange crystals of ∼10 mm maximum dimension were obtained by slow crystallization for about 1 day. Crystals were either kept in sealed containers in the mother liquor or selected and stored under N_2 in the presence of $CaCO_3$ as drying agent. The coloration of the crystals appears to depend on the content of nanoparticles of iron oxides. Exposure of the solution to air leads to darkening and crystallization of fine yellow needles of $(CH_3NH_3)Fe^{III}Cl_4$. Contamination by the latter can be avoided, while one can only reduce the amount of iron oxides, but they cannot be completely eliminated. Crystals all have the same habit with an aspect ratio of 6:4:1, and angles are 90°. Indexation using X-ray reveals that the long side

dx.doi.org/10.1021/ic402535u | *Inorg. Chem.* 2014, 53, 2068−2075

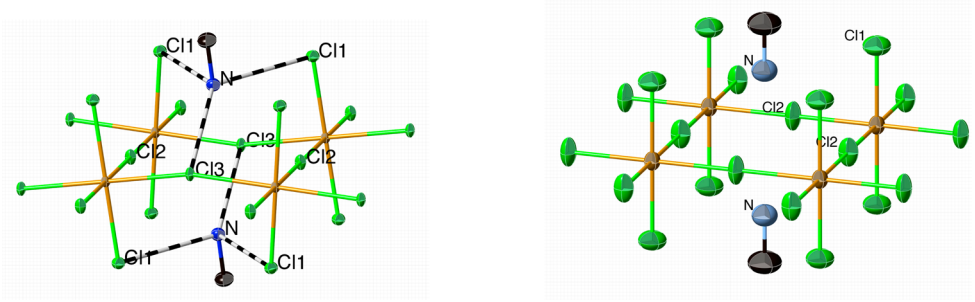

Figure 2. Docking of the organic methyl ammonium cations onto the inorganic layer in the *Pccn* (left, at 105 K) and *I*4/*mmm* (right, at 350 K) phases of MAFC. Hydrogen bonds are shown in white−black sticks.

corresponds to the crystallographic *b* axis, the short one to the *a* axis, and the plate to the *c* axis.

Thermal Measurements. Thermogravimetric analysis was performed on a SII EXSTAR TG/DTA 6200N from 300 to 600 K at a heating rate of 5 K/min under nitrogen flow. Differential scanning calorimetry was performed at different heating and cooling rates (2−40 K/min) in the range from 150 to 420 K using a Rigaku Thermoplus DSC8230.

Magnetic Susceptibility Measurements. All magnetic measurements were performed using Quantum Design SQUID magnetometers. The temperature dependence of the magnetic susceptibility $\chi(T)$ was measured between 2 and 400 K in different external fields from 50 to 5000 Oe. Isothermal magnetizations were measured in a field between ±50 kOe. Alternating current susceptibilities were measured in zero dc field and an ac field of 5 Oe oscillating at different frequencies between 10 and 1000 Hz. Powder samples were fixed in gelatin capsules for measurements, while selected single crystals were fixed on pieces of a drinking straw with Araldite. Angular dependence magnetization measurements were performed using the Quantum Design rotator. Crystals were indexed using X-ray diffraction prior to use.

Crystallographic Data Collections and Structure Determinations. Five single crystals from different batches were used for unit-cell determinations and structure refinements at different temperatures (Table S1, Supporting Information). Due to the layered structure it is not easy to cut large single crystals to sizes required for X-ray data collection. Any pressure applied to the crystals produces dislocations and consequently multicrystals. Finding small crystals from methanol solution is also problematic as the adhering solution forms a polycrystalline surface on drying, hampering the quality of data. We finally partially dissolved large crystals in alcohol to attain the crystal size required and placed them in oil before mounting. Typically a single crystal was mounted on a glass fiber. The temperature of the crystal was slowly decreased to 100 K (nitrogen flow cryostat) before taking measurements from 100 to 400 K. For one crystal data were taken at several fixed temperatures in both cooling and warming modes. Lattice parameters were measured as a function of temperature, and intensity data collections were made at some selected temperatures for which full structural analyses were carried out. All measurements were performed on a Bruker SMART-APEX diffractometer equipped with a CCD area detector and graphite-monochromated Mo Kα radiation, λ = 0.71073 Å, ω-scan mode (0.3° steps). Semiempirical absorption corrections on Laue equivalents were applied. Structures were solved by direct methods and refined by full-matrix least-squares against F^2 of all data using SHELX-97.[28] Non-hydrogen atoms were refined anisotropically. Hydrogen atoms were included with isotropic thermal parameters but not refined.

RESULTS AND DISCUSSION

Thermal Properties. Thermogravimetric analysis shows that MAFC is stable to 450 K, where it starts decomposing to give iron oxide. Differential scanning calorimetry shows a transition at 233 K with a very small hysteresis of ca. 2 K at a rate of 5 K/min increasing to 7 K for 20 K/min, suggesting a first-order phase transition. The second transition appears between 326 and 335 K with a hysteresis of ca. 9 K. These are consistent with reported birefringence and heat capacity data.[27]

Structures and Structural Phase Transitions. A detailed description of the structure of MAFC in all phases has not been properly reported, although several reports indicate it has a similar structure to that of the manganese analogue and is expected to follow the sequence of phase transitions derived for the family tree drawn by Heger et al.[20] We report the full structures at different temperatures covering the phase diagram (Figures 1 and 2). Using a Guinier camera and N_2-gas cryostat, Heger et al. found a transition from tetragonal to orthorhombic at 335 K and another from orthorhombic back to tetragonal at 233 K.[20] Our results from full structural determinations on single crystals do not agree with this conclusion. We find a change from tetragonal *I*4/*mmm* to orthorhombic *Pccn* at 335 K, but there is a continuous variation of the lattice and molecular parameters from 335 K through the 233 K transition down to 90 K without the previously observed transition at 233 K (Figure 3). Below 335 K the state is the same down to 90 K,

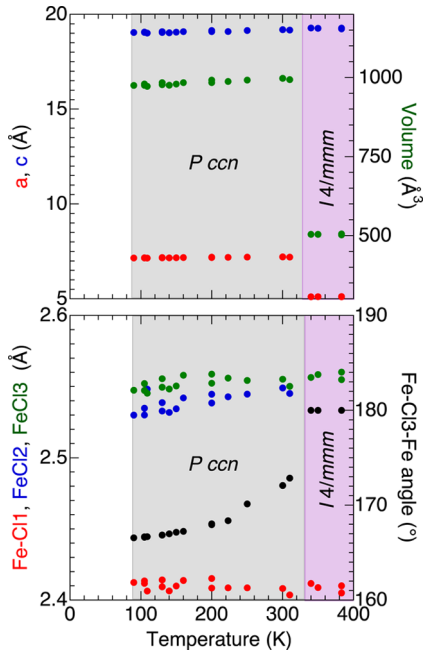

Figure 3. Structural phase diagram for MAFC: (top) lattice parameters, *a* (red), *c* (blue), and *V* (green) and (bottom) Fe−Cl1 (red), Fe−Cl2 (blue), and Fe−Cl3 (green) bond lengths and Fe−Cl3−Fe angle (black).

dx.doi.org/10.1021/ic402535u | Inorg. Chem. 2014, 53, 2068−2075

our lowest temperature X-ray measurement, below the magnetic ordering transition at 95 K. Lattice parameters increase marginally and linearly from 90 to 335 K, consistent with expansion as a function of increasing temperature. However, on close examination of the results we find a subtle tilting of the $FeCl_6$ octahedra accompanied by a puckering of the chlorine atoms within the layer from the tetragonal phase to the orthorhombic phase, and it is progressive down to 90 K (Figures 2 and 3).

Although MAFC exhibits several transitions in the temperature range under study, 2−400 K, the key features of the structure remain the same at all temperatures as that reported by Heger et al.[20] It consists of inorganic layers (*ab* plane) separated by double layers of organic cations stacked along the *c* axis. Each unit cell contains two staggered layers stacked in an *abab* fashion. The distance between two adjacent inorganic planes is ca. 9.5 Å. The inorganic layers are made up of corner-sharing octahedra of $FeCl_6$, as that in a perovskite. The octahedra display Jahn−Teller-compressed distortion where the nonbridging axial chlorine atoms are closer (Fe−Cl1 of 2.41 Å) than the intralayer bridging ones (Fe−Cl2 of 2.54 Å and Fe−Cl3 of 2.56 Å) to the iron center. The axial chlorine atoms are involved in hydrogen bonds with the ammonium moiety of the organic cations that sandwich the inorganic layer.

The principal differences in the structures are related to the cation−anion interactions involving the chlorine atoms and the hydrogen atoms of the ammonium forming Coulombic H bonds (Figure 1).[29] Given that there is a mismatch of symmetry, that is, the inorganic lattice is 4-fold and the methyl-ammonium is 3-fold, it is interesting to work out how the ordering of the organic cations takes place.[14] For the nonpolar phase at 383 K the iron and bridging chlorine are in the plane (Cl−Fe−Cl angles are all 90° and 180°) while the axial chlorine atoms are also at 90° from the bridging one. Consequently, the nitrogen atom is located exactly in the middle of the square of the coordinating metal−chlorine grid (N···Cl of 3.626 Å) with the ammonium group adopting several different but energetically equivalent orientations. An average of these positions is observed by diffraction, and an ordered network of hydrogen bonds is absent.

Below 335 K the 2D plane is progressively squeezed on lowering temperature, forcing the octahedra to tilt, taking the bridging chlorine atoms (Cl2) above and below the layer of iron atoms. The Fe atom sits in the plane. The Fe−Cl−Fe bridges are symmetrical, but now the bridging Fe−Cl3−Fe angle lowers gradually to 166.5° at 90 K. Interestingly, the Fe−Cl2−Fe angle remains close to 180°, and also the Cl1−Fe−Cl2 and Cl1−Fe−Cl3 angles are nearly 90°. The tilting takes place in pairs with two in and two out and propagates along the diagonal of the layer. The propagation is along 110 in one layer and along 1−10 for the other layer of the cell. This modification is accompanied by progressive displacement of the nitrogen atoms away from the middle of the square of the metal and chlorine atoms that surround it toward the two-in chlorine (Cl1) atoms pair (N···Cl1 of 3.30 Å) and away from the two-out pair (N···Cl1 of 3.87 Å). Interestingly, the bridging chlorine atom (Cl2) of the neighboring two-out pair moves toward the nitrogen atom (N···Cl3 of 3.26 Å). This leads to the three short connections (<3.4 Å) to the nitrogen atoms, removing any degeneracy, and complete order (Figure 2). Figure 4 shows the temperature dependence of the above-mentioned hydrogen-bond distances and their relations with the interatomic angles shown in Figure 3.

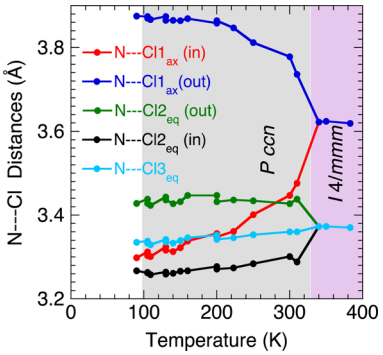

Figure 4. Temperature dependence of the Coulombic N···Cl interactions defining the docking of the ammonium cation onto the inorganic layer showing the progressive movement to the high-temperature structural transition (*Pccn* ⇔ *I*4/*mmm*).

Magnetic Properties and Magnetic Phase Transitions.

Magnetic susceptibility of a powdered sample was measured in an applied field of 5 kOe on cooling from 300 to 2 K (Figure S1, Supporting Information). Above 100 K the susceptibility exhibits a broad hump centered about 150 K, which is due to low-dimensional behavior within the layer. At 95 K a jump is observed, which is due to magnetic ordering. However, the presence of a jump and not a sharp decrease from the paramagnetic value has been responsible for the reported interpretations of a CAF ground state. Isothermal magnetizations at 2 and 90 K show linear dependence with the field except for in the latter a small hysteresis is observed. To elaborate on the question of the ground state we measured the temperature and field-dependence magnetic properties of 11 single crystals independently as a function of orientation in zero-field- (ZFC) and field-cooling (FC) modes and using both ac and dc methods. The picture that emerges is much more complex than the simple CAF reported. First, we uncovered a hidden-canting AF ground state involving at least four sublattices and MM in a relatively low critical field of 200 Oe (Figure 5).[30]

The results from several crystals were quite consistent and reproducible. We notice a few anomalies which are associated with the presence of bifurcation between ZFC and FC magnetizations which may be associated to the presence of

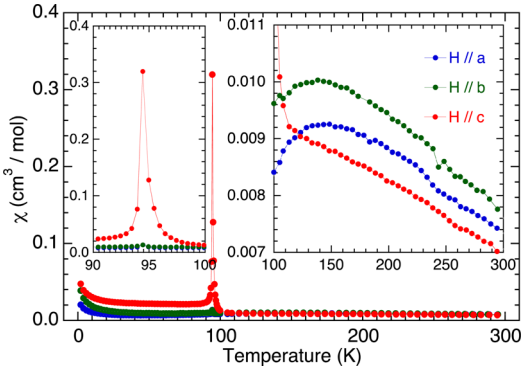

Figure 5. Temperature dependence of the magnetic susceptibility (*M*/*H*) on cooling in *H* = 50 Oe //*a* axis (blue), //*b* axis (green), and //*c* axis (red). (Insert) Zoom of the high-temperature region showing the low-dimensional behavior along the *a* and *b* axes (right), and zoom around the magnetic ordering temperature (left) showing the large anisotropy.

dx.doi.org/10.1021/ic402535u | Inorg. Chem. 2014, 53, 2068−2075

trace of particles of iron oxides and in one case a sharp rise below 3 K which we associate with long-range ordering (LRO) in the trivalent salt, $(CH_3NH_3)FeCl_4$,[31] also present in trace quantities. The superposed behavior for MAFC is very reliable. Data above 200 K were used to determine the Curie and Weiss constants in the paramagnetic region. The fits to the Curie–Weiss equation are rather poor and give a Curie constant ranging from 4.2 to 4.4 cm^3 K/mol and Weiss constant from −250 to −330 K for the different orientations. The Curie constant is about 25% higher than expected due to the presence of the iron oxide nanoparticles.

With a field of 50 Oe applied along the *a* or *b* axes, the magnetic susceptibility (Figure 5) behaves similarly and displays a broad hump centered at 150 K, though the absolute values are slightly different, suggesting a slight anisotropy in *g* values. A small anomaly is observed at T_N of 95 K in the FC data but is very weak in the ZFC data for each orientation. When the field is parallel to the *c* axis, the high-temperature susceptibility is almost linear and less than those for the *a*- and *b*-axis data. In contrast to the *a*- and *b*-axis measurements, that for *H*//*c* exhibits a very sharp peak in the susceptibility at 95 K. The increase becomes noticeable just above 100 K, well above T_N of 95 K, and the fall to 90 K reaches nearly the same value as that at 100 K. This suggests a ferromagnetic exchange component aligns the moments out of the plane just above T_N, and at the 3D Néel LRO the moment reduces to near zero, suggesting a fully compensated AF.[30] The results are in contradiction to those reported. In this orientation both ZFC and FC have the sharp peak but of slightly different magnitude.

By increasing the field applied for measurements of ZFC and FC (Figure 6), we notice considerable field dependence of the magnetization below T_N and very little changes above T_N. For *H*//*a*, the magnetization at the bifurcation point is enhanced by increasing the field. The ratio of FC magnetization to that of the ZFC reaches at most a factor of 2. For the different applied field the magnetization of FC deviates more from that for ZFC as the field is increased (Figure 6). For *H*//*c*, the behavior is more dramatic. In low applied field (50–200 Oe) the ZFC–FC almost overlap each other. As the field is increased to 300 Oe the ZFC peak slightly broadens while the magnetization in the FC reaches a saturation point. Further increase of the field broadens the ZFC magnetization peak even more and displays a prominent step at ca. 40 K up to a field of 410 Oe. The step is present in all samples studied. It is worth noting that the magnetization at 2 K in 5000 Oe is almost the same as those in 300–500 Oe, indicating a saturation point has been attained. This behavior is what is expected for a MM. Furthermore, the presence of the structure in ZFC data at ca. 40 K suggests we may have magnetic domains.

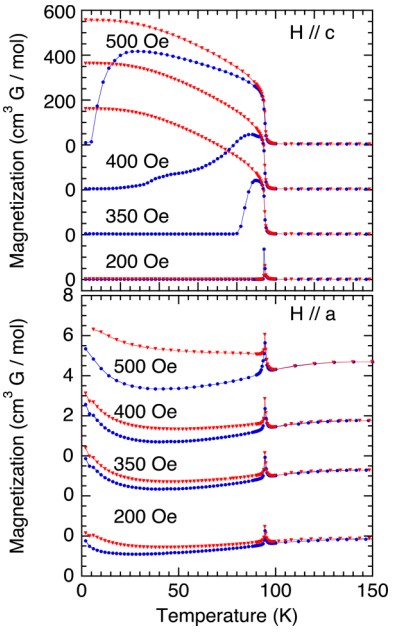

Figure 6. Temperature dependence of the magnetization in fixed field (200–500 Oe) for *H*//*c* (top) and *H*//*a* (bottom) in ZFC (blue dots) and FC (red triangles) modes. Note the offset of the magnetization in different fields.

Alternating current susceptibilities were measured for different frequencies (1–1000 Hz) in zero dc field and an oscillating field of 5 Oe (Figure 7). Two sharp peaks were observed at 94.7 and 94.5 K. There is very little frequency dependence. Interestingly, there are measurable changes in χ'' above T_N. Such observation suggests two changes in the system and also the presence of domains above T_N, possibly solely within the layers. As the temperature is lowered the coherent length of correlated moments will increase exponentially, generating pseudo large moments which interact with those in neighboring layers through dipole–dipole interaction to result in the 3D long-range ordering.[32] In this particular case, the ground state is an AF of fully compensated moments of all sublattices. Thus, the two anomalies are related to the 2D and 3D orderings of the moments.

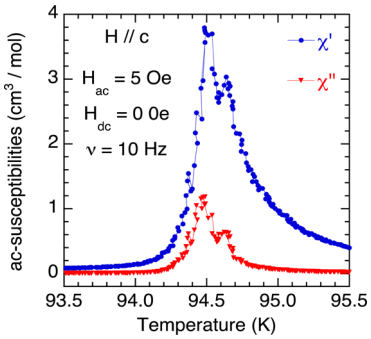

Figure 7. Temperature dependence of the ac susceptibilities, real part (blue) and imaginary part (red), for *H*//*c* around T_N.

Isothermal magnetizations at 2 K as a function of field for different orientations are shown in Figure 8. Hysteresis is observed for all three orientations, and also the ZFC virgin magnetization in each case is nearly zero. The latter means that a multidomain structure is present. For *H*//*a* or *b* axis, the hysteresis is nearly the same; the magnetization at saturation is lower than that for *H*//*a*. For *H*//*c* an almost square-shaped hysteresis is observed. However, for all orientations the magnetization increases linearly with field and does not reach saturation while the absolute values are only a small fraction of the expected saturation value for a fully aligned Fe(II) magnet ($M_{sat} = gS = 4\ \mu_B$). The result is consistent with a CAF state in $H > 200$ Oe. Using the remnant magnetization M_{rem} of 0.1 μ_B and $\alpha = \sin^{-1}(M_{rem}/M_{sat})$, we obtain a canting angle α of 1.4°. In addition, using a value of 0.2 μ_B in 5 T, we estimate the field can only fold the spin to 2.8°, thus indicating that the magnetic exchange anisotropy field will be very high, several hundreds of Tesla.

dx.doi.org/10.1021/ic402535u | Inorg. Chem. 2014, 53, 2068–2075

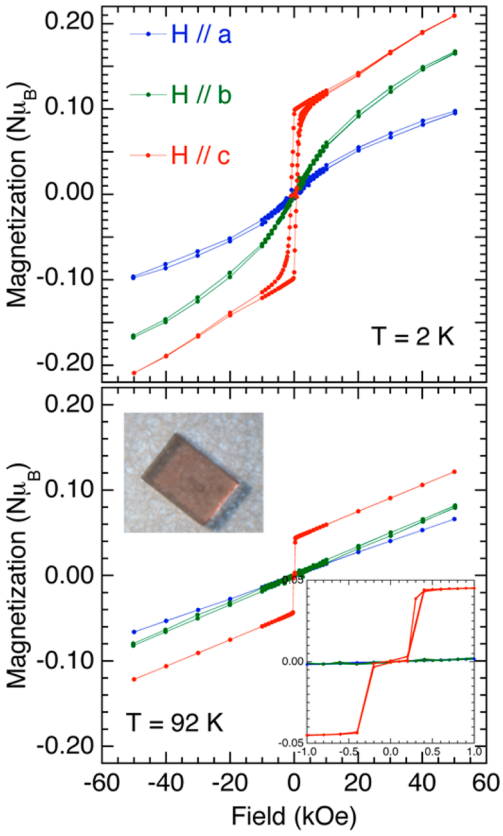

Figure 8. Isothermal magnetizations at two different temperatures, 2 (top) and 92 K (bottom), for $H//a$ (blue), $H//b$ (green), and $H//c$ (red). (Insert) Zoom of 92 K data to show the MM with the S-shaped field dependence magnetization and the crystal used for the measurements: short axis is a, long axis is b, and plate is c axis.

Isothermal magnetizations between 2 and 92 K show a very complex behavior akin those of $Co_2(OH)_2$terephthalate and Co_2(pyromellitate).[33] Just below T_N a MM behavior having a square S-shape is observed, and there is no hysteresis. As the temperature is lowered the square S-shape is retained and hysteresis starts to develop. With further decrease of temperature the coercive field, the remnant magnetization, and the magnetization at the maximum field increase. From the ZFC initial magnetization data we note the increase of the critical MM field as the temperature is lowered. Thus, as for $Co_2(OH)_2$terephthalate we can define the tricritical point of the MM to be when the hysteresis sets in at 85 K. Furthermore, we can define the MM transition field more accurately by performing a mutual induction experiment where we measure the ac susceptibilities as a function of field at fixed temperatures. We did this around T_N for 94.8, 94.6, and 94.4 K. At 94.8 K, the dc susceptibility is linear and both ac-susceptibility components are also linear, meaning we are in the paramagnetic state. At 94.6 K, a slight curvature for the dc magnetization and a broad hump in the real part of the ac susceptibility are seen at 150 Oe, indicating we are at T_N. At 94.4, an S-shaped dc magnetization and a very sharp peak are seen in both ac components at 200 Oe, which corresponds to the MM critical field at this temperature.

Using the critical MM field from the ZFC initial magnetization data and the remnant magnetization at different temperature we construct the magnetic phase diagram (Figure 9). It is clear that below the two lines we have a fully

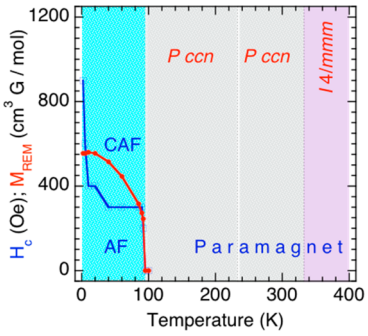

Figure 9. Magnetic phase diagram for MAFC: purple and gray regions ($I4/mmm$ and $Pccn$) are paramagnetic. Cyan region is the ordered magnetic state below T_N; blue line (H_c) divides AF and CAF. Red line is M_{rem}.

compensated AF, and above these lines it is a CAF. The paramagnetism exists above T_N at 95 K. From the ac susceptibility we also inferred the presence of superparamagnetism between ca. 100 and 95 K.

The refined magnetic data obtained using SQUID magnetometers and especially those obtained in low fields reveal a different picture of the ground state for MAFC. Taking the orientation, field, and temperature dependences of the magnetization into consideration, we propose the two magnetic structures for H < 200 Oe and H > 200 Oe (Figure 10).

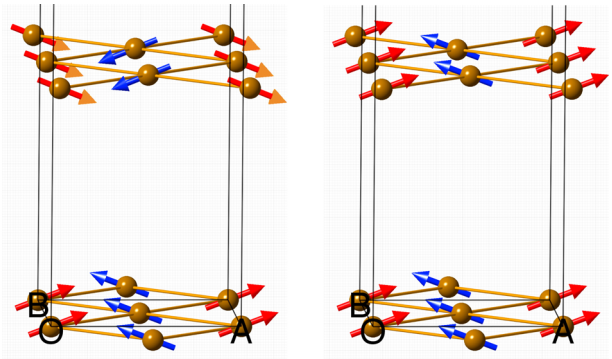

Figure 10. Proposed magnetic structures for MAFC for H < 200 Oe (left) and H > 200 Oe (right).

With two layers per cell two magnetic structures are possible for propagation vector k = 0, 0, 0, and only four magnetic sublattices (two per layer) are needed. Since the magnetization in the paramagnetic region is higher for a field parallel to the layer than perpendicular to it we can assume that the moments will lie in the plane; thus, it is an easy-plane magnet. Canting tends to take place along the intermediate axis that is perpendicular to the layers in the present case, that is, the c axis.[30] When the field is less than 200 Oe, ZFC and FC are almost the same for $H//c$, and it has the sharp peak. As we argued earlier, the sharp rise just above T_N is due to 2D weak ferromagnetism within each layer and the sharp fall is the 3D AF LRO having zero moment. As the field exceeds 200 Oe, the MM critical field, the moments are flipped to align with the field. Given the low M_{sat} value, only a fraction of the 4 μ_B expected for parallel alignment, we conclude that the MM state is a CAF. Thus, for low field the resulting canted moment of each layer cancels that of its neighbors, and in a field exceeding 200 Oe they are all parallel.

dx.doi.org/10.1021/ic402535u | Inorg. Chem. 2014, 53, 2068−2075

CONCLUSION

Re-examination of the crystallography of $(CH_3NH_3)_2FeCl_4$ and its temperature, field, and orientation dependence of the magnetic properties map a different structure phase diagram and reveals a fully compensated antiferromagnetic ground state consisting of four sublattices with a hidden canting which is transformed to a canted antiferromagnetic in a field greater than the metamagnetic critical field of 200 Oe. While the structural phase transition at 335 K involves a change from a tetragonal *I*4/*mmm* to an orthorhombic *Pccn* group, a subtle progressive concerted movement of the $FeCl_6$ octahedra and the methyl ammonium takes place, which introduces hydrogen bonding, satisfying 3- and 4-fold symmetries of the two moieties. The effect of using organic cations with different symmetry requirements will be very interesting for future understanding of the order−disorder transitions that may give rise to ferroelectricity and its effect on the magnetism.

ASSOCIATED CONTENT

Supporting Information

Magnetic susceptibility of a powder sample; isothermal magnetization at different temperatures; ac and dc field-dependence magnetization; summary of crystallographic data; description of the material included. This material is available free of charge via the Internet at http://pubs.acs.org.

AUTHOR INFORMATION

Corresponding Authors

*E-mail: kxi@hiroshima-u.ac.jp.
*E-mail: kurmoo@unistra.fr.

Notes

The authors declare no competing financial interest.

ACKNOWLEDGMENTS

This work was supported by a Grant-in-Aid (JSPS Fellows No. 20·6688, Scientific Research-A No. 18205023, Scientific Research-S No. 25220803, and exploratory research No. 19655050) from the Ministry of Education, Culture, Sports, Science and Technology (MEXT). This work was partly supported by a "Nanotechnology Support Project'" of MEXT and the Natural Science Center for Basic Research and Development (N-BARD), Hiroshima University. J.H. thanks Monkasho for a JASSO student scholarship, and M.K. thanks the CNRS, France.

REFERENCES

(1) (a) van den Brink, J.; Khomskii, D. I. *J. Phys.: Condens. Matter* **2008**, *20*, 434217/12. (b) Fiebig, M. *J. Phys. D: Appl. Phys.* **2005**, *38*, 123−152. (c) Cheong, S. W.; Mostovoy, M. *Nat. Mater.* **2007**, *6*, 13−20. (d) Hill, N. A. *J. Phys. Chem. B* **2000**, *104*, 6694−6709. (e) Ramesh, R. *Nature* **2009**, *46*, 1218−1219. (f) Eerenstein, W.; Mathur, N. D.; Scott, J. F. *Nature* **2006**, *442*, 759−765.

(2) (a) Kimura, T. *Ann. Rev. Mater. Res.* **2007**, *37*, 387−413. (b) Tokura, Y.; Seki, S. *Adv. Mater.* **2010**, *22*, 1554−1565.

(3) (a) Wang, Z.-M.; Zhang, B.; Fujiwara, H.; Kobayashi, H.; Kurmoo, M. *Chem. Commun.* **2004**, 416−417. (b) Wang, Z.-M.; Zhang, B.; Kurmoo, M.; Green, M. A.; Fujiwara, H.; Otsuka, T.; Kobayashi, H. *Inorg. Chem.* **2005**, *44*, 1230−1237. (c) Wang, Z.-M.; Zhang, Y.; Kurmoo, M.; Liu, T.; Vilminot, S.; Zhao, B.; Gao, S. *Aust. J. Chem.* **2006**, *59*, 617−628. (d) Zhang, B.; Wang, Z.-M.; Kurmoo, M.; Gao, S.; Inoue, K.; Kobayashi, H. *Adv. Funct. Mater.* **2007**, *17*, 577−585. (e) Wang, Z.-M.; Zhang, Y.; Liu, T.; Kurmoo, M.; Gao, S. *Adv. Funct. Mater.* **2007**, *17*, 1523−1536. (f) Wang, Z. M.; Zhang, B.; Zhang, Y. J.; Kurmoo, M.; Liu, T.; Gao, S.; Kobayashi, H. *Polyhedron* **2007**, *26*, 2207−2215.

(4) (a) Wang, X. Y.; Gan, L.; Zhang, S. W.; Gao, S. *Inorg. Chem.* **2004**, *43*, 4615−4625. (b) Wang, Z.-M.; Zhang, B.; Otsuka, T.; Inoue, K.; Kobayashi, H.; Kurmoo, M. *Dalton Trans.* **2004**, 2209−2216. (c) Wang, Z.-M.; Zhang, B.; Inoue, K.; Fujiwara, H.; Otsuka, T.; Kobayashi, H.; Kurmoo, M. *Inorg. Chem.* **2007**, *46*, 437−445. (d) Hu, K.-L.; Kurmoo, M.; Wang, Z.-M.; Gao, S. *Chem.—Eur. J.* **2009**, *15*, 12050−12064. (e) Wang, X. Y.; Wang, Z. M.; Gao, S. *Chem. Commun.* **2007**, 1127−1129.

(5) (a) Cui, H.; Zhou, B.; Long, L. S.; Okano, Y.; Kobayashi, H.; Kobayashi, A. *Angew. Chem., Int. Ed.* **2008**, *47*, 3376−3380. (b) Cui, H. B.; Wang, Z. M.; Takahashi, K.; Okano, Y.; Kobayashi, H.; Kobayashi, A. *J. Am. Chem. Soc.* **2006**, *128*, 15074−15075.

(6) (a) Jain, P.; Dalal, N. S.; Toby, B. H.; Kroto, H. W.; Cheetham, A. K. *J. Am. Chem. Soc.* **2008**, *130*, 10450−10451. (b) Jain, P.; Ramachandran, V.; Clark, R. J.; Zhou, H. D.; Toby, B. H.; Dalal, N. S.; Kroto, H. W.; Cheetham, A. K. *J. Am. Chem. Soc.* **2009**, *131*, 13625−13627. (c) Besara, T.; Jain, P.; Dalal, N. S.; Kuhns, P. L.; Reyes, A. P.; Kroto, H. W.; Cheetham, A. K. *Proc. Natl. Acad. Sci.* **2011**, *108*, 6828−6832. (d) Stroppa, A.; Jain, P.; Barone, P.; Marsman, M.; Perez-Mato, J. M.; Cheetham, A. K.; Kroto, H. W.; Picozzi, S. *Angew. Chem.* **2011**, *50*, 5847−5850. (e) Thomson, R. I.; Jain, P.; Cheetham, A. K.; Carpenter, M. A. *Phys. Rev. B* **2012**, *86*, 214304/7. (f) Li, W.; Zhang, Z.; Bithell, E. G.; Batsanov, A. S.; Barton, P. T.; Saines, P. J.; Jain, P.; Howard, C. J.; Carpenter, M. A.; Cheetham, A. K. *Acta Mater.* **2013**, *61*, 4928−4938.

(7) Xu, G. C.; Ma, X. M.; Zhang, L.; Wang, Z.-M.; Gao, S. *J. Am. Chem. Soc.* **2010**, *132*, 9588−9590.

(8) Sanchez-Andujar, M.; Presedo, S.; Yanez-Vilar, S.; Castro-Garcia, S.; Shamir, J.; Senaris-Rodriguez, M. A. *Inorg. Chem.* **2010**, *49*, 1510−1516.

(9) Zhang, W.; Xiong, R. G. *Chem. Rev.* **2012**, *112*, 1163−1195.

(10) (a) Kumagai, H.; Inoue, K. *Angew. Chem., Int. Ed.* **1999**, *38*, 1601−1603. (b) Inoue, K.; Imai, H.; Ghalsasi, P. S.; Kikuchi, K.; Ohba, M.; Ōkawa, H.; Yakhmi, J. V. *Angew. Chem., Int. Ed.* **2001**, *40*, 4242−4245. (c) Inoue, K.; Kikuchi, K.; Ohba, M.; Ōkawa, H. *Angew. Chem., Int. Ed.* **2003**, *42*, 4810−4813. (d) Imai, H.; Inoue, K.; Kikuchi, K.; Yoshida, Y.; Ito, M.; Sunahara, T.; Onaka, S. *Angew. Chem., Int. Ed.* **2004**, *43*, 5618−5621. (e) Imai, H.; Inoue, K.; Kikuchi, K. *Polyhedron* **2005**, *24*, 2808−2812. (f) Yoshida, Y.; Inoue, K.; Kurmoo, M. *Inorg. Chem.* **2009**, *48*, 10726−10736. (g) Higashikawa, H.; Okuda, K.; Kishine, J.; Masuhara, N.; Inoue, K. *Chem. Lett.* **2007**, *36*, 1022−1023. (h) Kishine, J.; Inoue, K.; Yoshida, Y. *Prog. Theor. Phys. Suppl.* **2005**, *159*, 82−95. (i) Numata, Y.; Inoue, K.; Baranov, N.; Kurmoo, M.; Kikuchi, K. *J. Am. Chem. Soc.* **2007**, *129*, 9902−9909.

(11) Ghalsasi, P. S.; Inoue, K. *Polyhedron* **2009**, *28*, 1864−1867.

(12) (a) Mitzi, D. B. *Prog. Inorg. Chem.* **1999**, *23*, 1−122. (b) Steadman, J. P.; Willett, R. D. *Inorg. Chim. Acta* **1970**, *4*, 367−371. (c) Arend, H.; Huber, W.; Mischgofsky, F. H.; K. Richter-van Leeuwen, G. *J. Cryst. Growth* **1978**, *43*, 213−223.

(13) Manaka, H.; Yamada, I.; Nishi, M.; Goto, T. *J. Phys. Soc. Jpn.* **2001**, *70*, 241−247.

(14) (a) Kind, R.; Roos, J. *Phys. Rev. B* **1976**, *13*, 45−54. (b) Kind, R.; Blinc, R.; Zeks, B. *Phys. Rev. B* **1979**, *19*, 3743−3754.

(15) (a) de Jongh, J.; Meidema, A. R. *Adv. Phys.* **1974**, *23*, 1−260. (b) Bellitto, C.; Day, P. *J. Mater. Chem.* **1992**, *2*, 265−271. (c) Day, P. *J. Chem. Soc., Dalton Trans.* **1997**, 701−705.

(16) (a) Polyakov, A. O.; Arkenbout, A. H.; Bass, J.; Blake, G. R.; Meetsma, A.; Caretta, A.; van Loosdrecht, P. H. M.; Palstra, T. T. M. *Chem. Mater.* **2012**, *24* (1), 133−139. (b) Cai, H.-L.; Yi Zhang, L.; Fu, D.-W.; Zhang, W.; Liu, T.; Yoshikawa, H.; Awaga, K.; Xiong, R.-G. *J. Am. Chem. Soc.* **2012**, *134*, 18487−18490.

(17) Baettig, P.; Oguchi, T. *Jpn. J. Appl. Phys.* **2010**, *49*, 080206/3.

(18) Mitzi, D. B. *J. Chem. Soc., Dalton Trans.* **2001**, 1−12.

(19) Guo, L.; Liu, H.; Dai, Y.; Ouyang, S. *J. Phys. Chem. Solids* **2007**, *68*, 1663−1673.

(20) (a) Knorr, K.; Jahn, I. R.; Heger, G. *Solid State Commun.* **1974**, *15*, 231−238. (b) Heger, G.; Mullen, D.; Knorr, K. *Phys. Status Solidi A*

1976, *35*, 627−637. (c) Geick, R.; Strobel, K. *J. Phys. C* **1977**, *10*, 4221−4239. (d) Arend, H.; Hofmann, R.; Waldner, F. *Solid State Commum.* **1973**, *13*, 1629−1632.
(21) Mostafa, M. F.; Semary, M. A.; Ahmed, M. A. *J. Magn. Magn. Mater.* **1980**, *15*−*18*, 448−450.
(22) Mostafa, M. F.; Semary, M. A.; Ahmed, M. A. *Phys. Lett.* **1977**, *61A*, 183−184.
(23) Mostafa, M. F.; Willett, R. D. *Phys. Rev. B* **1971**, *4*, 2213−2214.
(24) Willett, R. D.; Gerstein, B. G. *Phys. Lett.* **1973**, *44A*, 153−154.
(25) Nakajima, T.; Yamaguchi, H.; Goto, T.; Yoshizawa, M.; Suzuki, T.; Fujimura, T. *J. Magn. Magn. Mater.* **1983**, *31*−*34*, 1189−1190.
(26) (a) Keller, H.; Kündig, W.; Arend, H. *J. Phys. C* **1976**, *6*, 629−632. (b) Keller, H.; Kündig, W.; Arend, H. *Physica B* **1977**, *86*−*88*, 683−684.
(27) (a) Yoshizawa, M.; Suzuki, T.; Goto, T.; Yamakami, T.; Fujimura, T.; Nakajima, T.; Yamauchi, H. *J. Phys. Soc. Jpn.* **1984**, *53*, 261−269. (b) Yoshizawa, Y.; Goto, T.; Fujimura, T. *Phys. Rev. B.* **1982**, *26*, 1499−1502. (c) Goto, T.; Yoshizawa, M.; Tamaki, A.; Fujimura, T. *J. Phys. C* **1982**, *15*, 3041−3052. (d) Suzuki, T.; Yoshizawa, M.; Goto, T.; Yamakami, T.; Takahashi, M.; Fukimura, T. *J. Phys. Soc. Jpn.* **1983**, *52*, 1669−1675.
(28) (a) Sheldrick, G. M. *SHELXL-97, Program for the Solution of Crystal Structures from X-Ray Data*; University of Göttingen: Germany, 1997. (b) Sheldrick, G. M. *Acta Crystallogr., Sect. A* **2008**, *64*, 112−122.
(29) Jeffery, G. A. *An Introduction to Hydrogen Bonding*; Oxford University Press: Oxford, 1997.
(30) Herpin, A. *Theorie du Magnétisme*; Presse Universitaire de France: Paris, 1968.
(31) Lammers, E.; Verstelle, J. C.; van Duyneveldt, A. J.; Lowe, C.; Carlin, R. L. *J. Phys., Colloq. C8* **1988**, *49*, 1465−1466.
(32) In *Magnetic properties of layered transition metal compounds*; de Jongh, L. J., Ed.; Dordrecht: Kluwer, 1990.
(33) (a) Kurmoo, M. *Philos. Trans. A* **1999**, *357*, 3041−3061. (b) Kurmoo, M.; Kumagai, H.; Green, M. A.; Lovett, B. W.; Blundell, S. J.; Ardavan, A.; Singleton, J. *J. Solid State Chem.* **2001**, *159*, 343−351. (c) Kumagai, H.; Kepert, C. J.; Kurmoo, M. *Inorg. Chem.* **2002**, *41*, 3410−3422. (d) Kurmoo, M. *Chem. Soc. Rev.* **2009**, *38*, 1353−1379.